Mon. Not. R. astr. Soc. (1977) **179**, 189–207

Coherent pulsar radio radiation by antenna mechanisms: general theory

Gregory Benford and Robert Buschauer *Physics Department, University of California, Irvine, California 92717, USA*

Received 1976 July 30; in original form 1976 June 15

Summary. We apply our general formalism for coherent curvature radiation to the radio emission of pulsars. We adopt the magnetospheric model of Ruderman & Sutherland. The electrostatic streaming instability dominates all other plasma modes. The beam–plasma instability they envisioned does not grow rapidly enough to produce appreciable coherence, and thus cannot explain the observed radiation. Nonetheless, we derive an expression for pulsar luminosity, $L(\nu) \propto \nu^{-2.2}$, with features which should be shared by a general class of simple, instability-driven radiation models. The electrostatic instabilities make the electron–positron plasma into a phased array, like an antenna. This proves much more efficient than the usual, local picture of coherence which extends only over one wavelength. We also conjecture that the high-frequency steepening of $L(\nu)$ derives from linear growth near the pulsar, and that the low-frequency turnover may arise when relativistic plasma energy density exceeds the dipolar field energy density, rather than from self-absorption. In Tables 1 and 2 we give convenient conversions from observed radiation properties to pulsar parameters in hopes that these will prove useful to observers.

1 Introduction

It is widely assumed that radiation from pulsars comes from coherent relativistic processes. There are at least two good reasons to believe this: the brightness temperature in the radio wavelengths is $\sim 10^{30}$ K, and the signal displays erratic behaviour on a scale far faster than the pulse width. (For a review, see Ginzburg & Zheleznyakov 1975). Gradually, more detailed models of the pulsar magnetosphere have emerged (Holloway 1975) until at the moment, the most convincing picture is that afforded by the work of Ruderman & Sutherland (1975). They ascribe the radiation to coherence induced by a specific beam-plasma instability in the pulsar magnetosphere, following ideas of Sturrock (1971).

Recently we have developed a general formalism for coherent emission (Buschauer & Benford 1976) for any plasma system moving along curved trajectories, assuming the plasma is perturbed by a plane wave of wave number k and coherence length s_0. This longitudinal

electrostatic wave causes particle bunching, which orders the phases of emitting particles. When $ks_0 \gg 1$ the emitted radiation peaks strongly at the plasma wave frequency. Only when the plasma wave is at rest in the plasma frame – that is, the wave is not convective in that frame – does the coherent spectrum factor into a form which is often assumed, i.e. a product of the single particle spectrum and a resonance function in ks_0, times the square of the number of coherent particles, N^2. When the plasma wave is convective, as is the case for many streaming instabilities, no simple functional form emerges. This is precisely the case for the radiation picture touched upon, but not worked out, by Ruderman & Sutherland.

They envision an electron–positron plasma of density $n_p \approx 10^{14}\,\mathrm{cm}^{-3}$ near the pulsar surface, which streams outward after it is created above a magnetospheric gap at the pulsar pole. A distribution of faster positrons ($n_b \approx 7 \times 10^{10}\,\mathrm{cm}^{-3}$, $\gamma_b \approx 10^6$) streams through this electron–positron plasma, causing a convective beam–plasma instability. This situation is covered by the convective case in our theory. Within the framework of the Ruderman–Sutherland model as it stands, this is the most obvious source of instability.

However, we shall find that this mode cannot yield appreciable radiation because the growth rate given by Ruderman & Sutherland contains an algebraic error. Compare our growth time τ of Table 1, (m) with Ruderman & Sutherland's equation (55); they differ by a factor of $\gamma_\pm^{1/2}$. Since $\gamma_\pm \approx 800$, this is an important difference. Also, τ varies with distance from the pulsar, r; to find the total e-foldings of a wave we must integrate over r; Ruderman & Sutherland simply took the maximum τ. We find that the combined effect of the $\gamma_\pm^{1/2}$ and averaging over r reduces total growth by $\sim 10^{-2}$ from the Ruderman–Sutherland result. The correct form appears in the exponential of equation (11). The correct τ is far too low to give appreciable bunching before the plasma escapes from the pulsar magnetosphere. Thus this beam–plasma mode cannot yield appreciable radiation unless the plasma wave is stimulated very near the pulsar – that is, a large-amplitude wave must be launched from near the polar cap region. There appears to be no clear reason why such a large-amplitude wave should arise and indeed, to advocate one is to go athwart the basic motive – i.e. looking for unavoidable waves which grow spontaneously from background noise. Thus, the Ruderman–Sutherland picture must be wrong in some facet; it cannot explain the coherent radiation.

This does not mean the overall Ruderman–Sutherland *dynamical processes* are wrong, though. The formation of a gap above the pulsar pole, and the resultant sparking, seems a reasonable picture. It may be possible to allow some additions to the Ruderman–Sutherland picture, for example ion beams – which make some types of beam–plasma instability very rapid. These instabilities may provide the necessary particle coherence for radiation.

Thus, in this paper we shall use the basic picture of Ruderman & Sutherland to derive an expression for the luminosity of radio pulsars, assuming their beam–plasma mode grows from noise. The formalism displays several features which must be shared by *any* reasonably simple instability-driven radiation. Our radiation formulae differ significantly from the single-particle form because the plasma wave is relativistic in the frame of the emitting plasma; the added acceleration from this wave oscillation alters the radiation pattern. We picture the dense plasma, which is rippled by the passing plasma wave, as a *phased array* like an actual antenna. An electromagnetic wave launched along the (very nearly straight) array finds, after it has travelled a wavelength, that the plasma electrons near it are still in phase with it, because they are driven by the electrostatic wave of the same wavelength. Thus all emissions add coherently.

Our aim in this paper is to follow through a particular plasma instability as far as possible, calculating the luminosity, and show how much can be extracted from basic plasma physics. Though the particular instability fails to explain the data because it does not grow rapidly enough, the development of the problem gives a programmatic way to modify the calcula-

Table 1.

Physical quantity	Analytic expression	R–S equation no.	
(a) Radius of curvature of dipolar field lines; the equality applies to last open field lines	$\rho \geqslant 1.4 \times 10^9 r_8 P^{1/2}$ cm	46	10^9 cm
(b) Maximum primary positron energy normalized to its rest mass	$\gamma_{max} = 3 \times 10^6 \rho_6^{4/7} \frac{1}{P^{1/7} B_{12}^{1/7}}$	22 + 42	3×10^6
(c) Maximum primary (beam) number density	$n_b = \frac{B_s^d}{Pec}\left(\frac{r_p}{r}\right)^3$	50	$7 \times 10^{10}(10^6/r)^3$ cm^{-3}
(d) Relativistic factor of electron–positron plasma with respect to pulsar	$\gamma_\pm = 840 \frac{\rho_6^{5/7}}{B_{12}^{3/7} P^{3/7}}$	—	840
(e) Relativistic factor of primarys with respect to pulsar	$\gamma_b \leqslant \gamma_{max}$	—	10^6
(f) Maximum secondary (plasma) number density	$n_p = \frac{\gamma_{max}}{2\gamma_\pm}\frac{B_s^d}{ecP}\left(\frac{r_p}{r}\right)^3$	51	$10^{14}(10^6/r)^3$ cm^{-3}
(g) Relation of beam number densities in pulsar and plasma frames	$n'_b = \frac{1}{2\gamma_\pm} n_b$	54c	$n'_b = 6 \times 10^{-4} n_b$
(h) Relation of electron–positron number densities in their rest and pulsar frames	$n'_p = \frac{1}{\gamma_\pm} n_p$	54a	$n'_p = 1.2 \times 10^{-3} n_p$
(i) Relation of beam relativistic factor in plasma and pulsar frames	$\gamma'_b = \frac{1}{2\gamma_\pm}\gamma_b$	54b	$\gamma'_b = 6 \times 10^{-4}\gamma_b$
(j) Plasma frequency in plasma frame	$\omega'_p = \left(\frac{4\pi n'_p e^2}{m}\right)^{1/2}$	53b	$2 \times 10^{10}(10^6/r)^{3/2}$ s
(k) Beam plasma frequency in plasma frame	$\omega'_b = \left(\frac{4\pi n'_b e^2}{\gamma'^3_b m}\right)^{1/2}$	53c	$3 \times 10^4 (10^6/r)^{3/2}$ s
(l) Cyclotron frequency in plasma frame	$\omega'_c = \frac{eB_s^d}{mc}\left(\frac{r_p}{r}\right)^3$	—	$2 \times 10^{19}(10^6/r)^3$ s
(m) Growth time of fastest growing mode of the unstable beam–plasma spectrum $\equiv 1/\Gamma(k^*)$	$\tau = \frac{\gamma_b \gamma_\pm^{1/2}}{2}\left(\frac{\gamma_\pm}{\gamma_{max}}\right)^{1/6}\left(\frac{mcP}{eB_s^d}\right)^{1/2}\left(\frac{r}{r_p}\right)^{3/2}$	—	$5 \times 10^{-4}(r/10^6)^{3/2}$ s
(n) Relation of growth time (see m) in plasma and pulsar frames	$\tau = \gamma_\pm \tau'$	55	$\tau = 800\tau'$
(o) Dipole field strength	$B^d = B_s^d\left(\frac{r_p}{r}\right)^3$	—	$10^{12}(10^6/r)^3$

Notes to Table 1:

Where

$r_s \equiv$ distance (in units of 10^8 cm) from pulsar centre to observation point.

$P \equiv$ pulsar period/s.

$\rho_6 \equiv$ radius of curvature (in units of 10^6 cm) of field lines near pulsar surface.

$r_p \equiv$ pulsar radius $\approx 10^6$ cm.

$B_s^d \equiv$ surface component of dipole field at cap $\approx (1-3) \times 10^{12}$ G.

$B_{12} \equiv B_s^d 10^{-12}$.

Primed quantities refer to plasma frame whereas unprimed quantities refer to pulsar frame.

In expression (l) we set $B^d \equiv (B^d)'$ since the magnetic field is locally along the direction of motion of the beam plasma column (Jackson 1962).

To obtain numerical values we set $P = 1$ s, $B_s^d = 10^{12}$ G.

tion, once a better instability is known. Thus, for example, should an *ion* streaming instability eventually prove reasonable after a detailed study of the sparking phenomena, our methods can be applied with straightforward modifications to yield the luminosity and other spectral features.

2 Unstable beam–plasma modes in a strong magnetic field

Consider a cold, relativistic electron beam propagating along a magnetic field through a cold, stationary plasma. The system is assumed to be charge and current neutral. If we confine ourselves to the strong field ($\omega_c \geqslant 3\omega_p$), weak beam ($n_b/\gamma n_p \ll 1$) case, then there are four unstable modes in the electrostatic approximation (Godfrey, Shanahan & Thode 1975). We have defined $\omega_c \equiv |e|B_0/mc$, $\omega_p^2 \equiv 4\pi n_p e^2/m$, $n_p \equiv$ plasma density, $n_b \equiv$ beam density, $\gamma \equiv (1 - V_{beam}^2/c^2)^{-1/2}$. A crude criterion for the dominance of the two stream is that its linear growth rate exceed that of the other instabilities by at least a factor of 3/2. Using the well-known maximum growth rates (Godfrey *et al.* 1975) we write the conditions for dominance of the two stream over the hybrid two stream, electron cyclotron and upper hybrid instabilities, respectively, as

$$\frac{\omega_c}{\omega_p} \geqslant 3,$$

$$\frac{\omega_c}{\omega_p} \geqslant \frac{1}{2^{1/3}3^{1/2}}\gamma^2\left(\frac{n_b}{n_p}\right)^{1/3}, \tag{1}$$

$$\frac{\omega_c}{\omega_p} \geqslant \frac{\sqrt{3}}{2^{2/3}}\gamma\left(\frac{n_b}{n_p}\right)^{1/6}.$$

Numerical solution of the full electromagnetic dispersion relation (Godfrey *et al.* 1975) for the above system confirms the frequencies and growth rates predicted by the electrostatic analysis with one exception: the two-stream spectrum is much narrower in angle; *it is essentially one dimensional.*

In a later section we shall find that the two stream dominates the others in pulsar environments. Therefore, we now briefly summarize a few of its salient features. The one-dimensional electrostatic dispersion relation, $1 - \omega_p^2/\omega^2 - \omega_b^2/\gamma^3(\omega - kV_0)^2 = 0$ admits a spectrum of unstable solutions in k. We have used $\omega_b^2 \equiv 4\pi n_b e^2/m$ and $V_{beam} \equiv V_0$. The fastest growing mode has wavenumber $k^* = \omega_p/V_0$ and growth rate

$$\Gamma = \frac{3^{1/2}}{2^{4/3}}\frac{1}{\gamma}\left(\frac{n_b}{n_p}\right)^{1/3}\omega_p.$$

3 Dominance of the two-stream instability in pulsars; single wave model

3.1 PULSAR MODEL

We adopt the Ruderman–Sutherland (1975) model for pulsars. In view of Holloway's criticisms of other models (1975), it seems the Ruderman–Sutherland model is probably the only reliable detailed view currently available.

The radio-emitting region is the volume occupied by the section of open field lines between the pulsar surface and $r \approx 5 \times 10^9$ cm from the surface. (We present a detailed discussion of the inner and outer boundaries in a later section.) For calculational simplicity we assume the magnetization and rotation axes are nearly antiparallel. Within the above volume, columns of relativistic ($\gamma_\pm \approx 800$) electron–positron plasma of length $d \sim 3 \times 10^5$ cm move out along tubes of curved, open field lines. Each column is pervaded by a stream of high-energy ($\gamma_b \approx 10^6$) positrons. The perpendicular temperature is assumed small because: (1) the charged particles radiate away their perpendicular energy quickly in the strong ambient B-field by the synchrotron mechanism; (2) the system cools transversely as it moves along the field lines due to the adiabatic invariant ($W_\perp/B^2$). Table 1 presents a list of commonly used quantities and their numerical values. Primes denote the plasma frame whereas unprimed quantities are taken in the pulsar frame.

3.2 UNSTABLE MODES IN PULSARS

The environment described above is a beam–plasma system subject to the instabilities described previously. Equation (1) defines the conditions for the dominance of the two-stream mode. We apply these conditions in the plasma rest-frame, use the values listed in Table 1, and let $B_{12} = 1$, $\rho_6 = 1$ and $\gamma_b = 10^6$. The two stream dominates if

(a) $$3 \times 10^8 \geqslant \left(\frac{r}{r_p}\right)^{3/2} \frac{1}{P^{1/7}},$$

(b) $$5 \times 10^6 \geqslant \left(\frac{r}{r_p}\right)^{3/2} P^{5/21},$$

(c) $$7.6 \times 10^4 \geqslant \left(\frac{r}{r_p}\right)^{3/2} P^{13/21}.$$

For the fastest pulsar $P \approx 10^{-3/2}$ s and condition (a) is trivially satisfied for all r of interest. Similarly (b) holds for $r \leqslant 2.5 \times 10^{10}$ cm (when $P = 4$ s) which includes the entire range of interest. For the slowest pulsar the last condition (that the two-stream growth rate dominate the electron–cyclotron growth rate) is only satisfied out to $r \approx 10^9$ cm. However, consider the following arguments: (1) For most pulsars $P < 4$ s so condition (c) is satisfied to larger r. (2) Ruderman & Sutherland assert that $r \sim 5 \times 10^9$ cm is the maximum distance to which beam–plasma instabilities can be excited. The actual distance may be significantly smaller. Therefore, the two stream may dominate over the entire unstable range in r. (3) The reader is reminded that the equality in (c) simply means that the growth rate of the two stream is 3/2 times as large as that of the electron cyclotron. Since the two stream has grown faster than the cyclotron mode for $r \leqslant r_c \equiv 1.8 \times 10^9 P^{-26/63}$, the amplitude of the former will continue to dominate the latter to distances greater than r_c. This argument is strengthened by the fact that the growth rates *decrease* with time because the system is following diverging field lines, and plasma densities decline as r^{-3}. This increases the time required for the electron–cyclotron instability to catch up to the two stream. (4) The electron–cyclotron instability is probably more sensitive to transverse beam temperature stabilization than is the two stream (Thode 1973). In the spirit of the above discussion we consider only the charge bunching due to the two-stream instability in what follows. Furthermore, since $\omega_c'/\omega_p' \gg 3$ the linear interaction will be effectively one dimensional.

3.3 COHERENCE LENGTH AND SINGLE WAVE MODEL FOR PULSARS

Section 3.2 shows that the electron–positron plasma charge bunching is due primarily to the presence of one-dimensional electrostatic waves. A detailed knowledge of the genesis of the unstable spectrum is lacking. However, there may exist a preferential excitation of modes in the plasma near the fastest growing two-stream wavenumber, k^*, due to the two-stream electric fields of nearby sparks. Under such circumstances we describe the evolution of the wave spectrum by solving the linearized fluid and Poisson equations for a one-dimensional, beam–plasma system, as an initial value problem. Following the technique of Mikhailovskii (1974) and assuming the initial density perturbations of the beam and plasma to be proportional to $\exp(-z'^2/4b'^2)\exp(ik^*z')$ in the plasma rest frame, we find that so long as $b \gg 20\,\mathrm{cm}/\sqrt{k^*(\mathrm{cm}^{-1})}$ (which is not unduly restrictive),

(1) The peak of the wave-packet envelope moves only a small fraction of the effective length of the packet during the time, $t_e = \rho/\gamma_\pm c$, required to emit radiation in the direction of a distant observer;

(2) The fractional change in the width of the packet is small during radiation time t_e:

(3) The growth time of the fastest growing instability is long compared to t_e;

(4) The phase of the wave packet departs negligibly from that of a pure harmonic wave over the effective extent of the packet.

Therefore, we are led to consider the following 'idealized wave-packet' model.

The electric field *in the plasma frame* is represented by a simple harmonic wave of length s_0' whose frequency and wavenumber are those of the fastest growing mode of the one-dimensional two-stream spectrum:

$$E_1'(z', t') = E_0' \sin[k^*z' - \omega_r^{*\prime} t'] \quad \text{for} \quad |z'| \leqslant \frac{s_0'}{2}. \tag{2}$$

Since the amplitude of a longitudinal electric field and the phase of a plane wave are both Lorentz invariants, we have in the pulsar frame

$$E_1(z, t) = E_0' \sin(k^*z - \omega_r^* t); \quad ut - \frac{s_0}{2} \leqslant z \leqslant ut + \frac{s_0}{2}. \tag{3}$$

At present the only lower bound on s_0 is that set by the condition $s_0 \gg 20/\sqrt{k^*}$ cm. However, other factors such as radiation reaction or different initial conditions from the ones considered may increase s_0. Furthermore, unless $s_0 \gg \lambda^*$ the concept of a plasma wave ceases to be meaningful. Finally, the high radio brightness temperatures of pulsars ($\sim 10^{30}$ K) imply the existence of an efficient coherent emission mechanism, so plasma charge bunching is extensive and s_0 is large.

4 Spectral power distribution from pulsars

4.1 FORMAL SPECIFICATION OF THE SYSTEM

The maximum radial width of a monoenergetic plasma column (for the emission of coherent curvature radiation) is limited by corotation effects. The position lag along the direction of motion between two highly relativistic monoenergetic particles travelling along adjacent curved field lines is $\Delta s = (c\Delta t/\rho)\Delta\rho$, where $\Delta\rho$ is the radial separation of the trajectories, ρ is the average radius of curvature, and Δt is the time over which the lag Δs occurs. The particles remain coherent over a radiation time $\Delta t = t_e = \rho/\gamma_\pm c$ if $\Delta s/\lambda \ll 1$, where λ is the observed radiation wavelength. This implies that $\Delta\rho \approx \gamma_\pm \lambda$ is an upper bound on the effective radial width.

The physical system we consider, then, is as follows: a beam–plasma column moves along a tube of curved field lines (whose local radius of curvature is ρ_0), above a pulsar polar cap. The length of the column is 3×10^5 cm, the radial width $\xi_0 \ll 800\lambda$ and the third dimension, η_0, simply satisfies the condition $\eta_0 \ll \rho_0$. The unstable spectrum is dominated by the fastest growing mode of the one-dimensional, two-stream interaction. This mode causes plasma charge bunching and thus coherent curvature radiation. We therefore represent the electric field in the plasma rest frame by equation (2). The density and radius of curvature vary along the system trajectory because the system follows diverging dipolar field lines. However, these quantities do *not* change appreciably over a radiation time t_e; so we calculate the radiation emitted in the direction of a distant observer assuming constant ρ, Γ, n_p, n_b etc. Later, when we sum the contribution of many plasma columns it will be necessary to consider the effects of spatial variations in ρ and n.

To calculate the coherently emitted radiation by a bunched plasma column we require an expression for the perturbed current density in the pulsar frame. The current and charge densities of the plasma (in the plasma frame) due to the single wave are

$$J' = \sum_{\substack{\text{plasma} \\ \text{species}}} q_\alpha n'_{\alpha 0} V'_{\alpha 1}; \quad \rho' = \sum_{\substack{\text{plasma} \\ \text{species}}} q_\alpha n'_{\alpha 1}$$

where $n'_{\alpha 1}$ and $V'_{\alpha 1}$ are found from the linearized fluid and Poisson equations.

After carrying out the transformation to the laboratory frame, $J = \gamma_\pm [J' + c\rho']$, we find

$$J = \hat{z} J_0 \sin [k^* z - \omega_r(k^*) t]; \quad ut - \frac{s_0}{2} \leqslant z \leqslant ut + \frac{s_0}{2}, \tag{4}$$

where

$$J_0 = - \frac{2 |e|^2 E'_0 n'_p \gamma_\pm \exp(N)}{m \omega'_r(k^{*\prime})}$$

and $\omega'_r(k^{*\prime})$ is the real part of the mode frequency in the plasma frame, N is the number of e-foldings that occurrs since onset.

If the centre of momentum of the cold plasma moves along a curved trajectory of radius ρ_0, then equation (4) becomes

$$\mathbf{J} = \hat{\phi}(\phi) J_0 \sin(k^* \rho_0 \phi - \omega^* t); \quad \phi_0 - \frac{\alpha_0}{2} \leqslant \phi \leqslant \phi_0 + \frac{\alpha_0}{2}, \tag{5}$$

where α_0 is the angular width of the column, ϕ is the conventional cylindrical coordinate, and $\phi_0 = ut/\rho_0$.

4.2 COHERENT RADIATION FORMALISM

Recently, we have given a detailed formalism describing the coherent curvature radiation from the current density expression equation (5) (Buschauer & Benford 1976). Fig. 1 describes the system under consideration. The centre of momentum moves in the x, y plane along a curve of radius ρ_0; $\hat{n}$ is a unit vector in the direction of observation and lies in the x, z plane. The radial width of the system is ξ_0; the height is η_0 and the length as observed in the x, y, z (pulsar) frame is $s_0 = \alpha_0 \rho_0$. The plasma moves with relativistic factor $\gamma_\pm \equiv (1 - u^2/c^2)^{-1/2} \gg 1$.

If $d^2 I_{\text{single tube}}/d\omega\, d\Omega$ is the energy radiated per unit solid angle $d\Omega$ in the direction of $\hat{n}$,

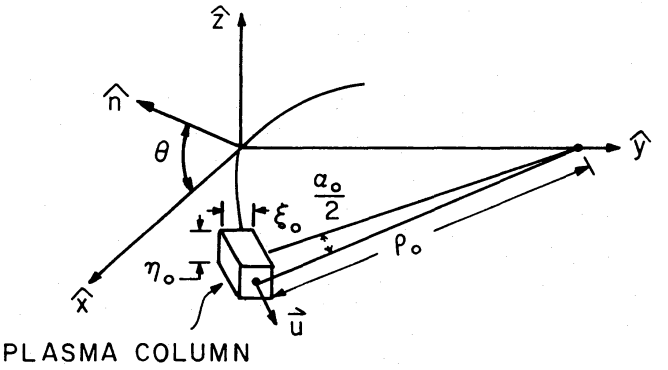

Figure 1. Geometry for performing coherent curvature radiation calculation.

per unit frequency $d\omega$, by a single plasma column, then

$$\frac{d^2I}{d\zeta\, d\omega} = \int_{-\infty}^{\infty} d\theta\, \frac{d^2 I_{\text{single tube}}}{d\omega\, d\Omega} \tag{6}$$

is the energy radiated per unit plane angle in the xy plane around the x axis per unit frequency interval as the relativistic plasma column passes by. For the streaming instability the phase velocity of the wave in the plasma frame is about c, so (Buschauer & Benford 1976)

$$\frac{d^2I(\omega)}{d\zeta\, d\omega} = \frac{1}{2.3^{1/3}\Gamma(1/3)} (J_0 s_0 \xi_0 \eta_0)^2 \frac{\sin^2[(k^* - k)s_0/2]}{[(k^* - k)\, s_0/2]^2} \frac{k^{1/3}\rho_0^{1/3}}{c^3}, \tag{7}$$

valid if $k\eta_0/2 \leqslant \gamma_\pm/10$, $k^*\rho_0/\gamma_\pm^3 < 50$.

We now use (7) to calculate the spectral energy distribution emitted from a pulsar polar cap.

Initially, we consider the idealized situation in which the spin angular momentum ($\boldsymbol{\Omega}$) and magnetization axes are antiparallel. Hence the polar cap is circular and there is rotational symmetry about these axes. Furthermore, we assume that the magnetic field lines are strictly dipolar over the radiating region. In reality we expect that $\mathbf{M}$ and $\boldsymbol{\Omega}$ are not aligned and the polar cap is not circular. We discuss this matter later.

Choose a unit vector $\hat{n} = \hat{x}\sin\mu_0 + \hat{z}\cos\mu_0$ fixed in the pulsar, to define the direction in which to monitor the emitted radiation (see Fig. 2).

First we sum the contributions to the energy emitted into a solid angle $d\Omega$ along $\hat{n}$ by all tubes of field lines characterized by the same value of $D = r/\sin^2\alpha$, where r is the distance

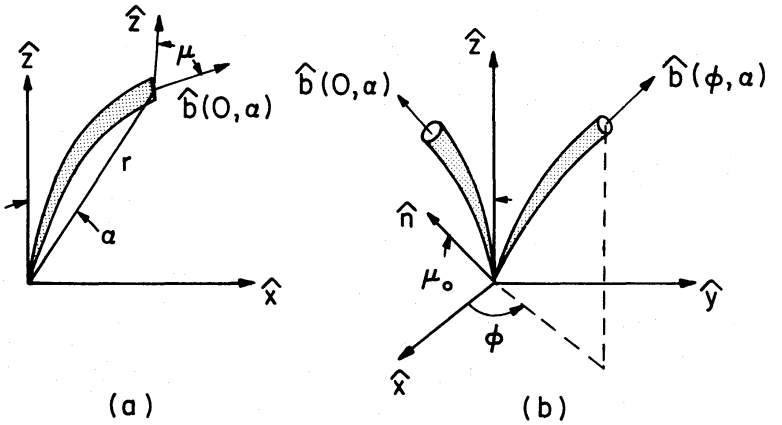

Figure 2. Dipolar tubes of force emanating from pulsar polar cap. The pulsar is at the origin.

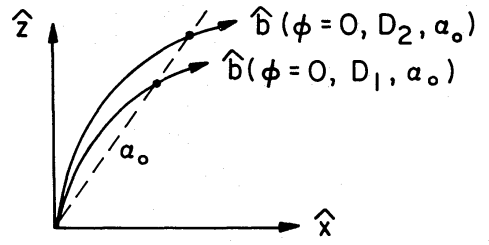

Figure 3. Illustration of field lines with different values of D.

from the pulsar centre and α is the corresponding polar angle (see Figs 2 and 3). The result of a simple calculation is

$$\frac{d^2I_D}{d\omega\, d\Omega(\hat{n})} = \frac{\sin\alpha_0}{\sin\mu_0}\frac{r}{\eta_0(r,\alpha_0)}\frac{(J_0 s_0 \xi_0 \eta_0)^2}{2.3^{1/3}\Gamma(1/3)}\frac{\sin^2[(k^*-k)\,s_0/2]}{[(k^*-k)\,s_0/2]^2}\frac{k^{1/3}\rho_0^{1/3}}{c^3} \tag{8}$$

where $\mu_0 = 3/2\,\alpha_0$ if $\alpha_0, \mu_0 \ll 1$; otherwise $\cos\mu_0 = (1 - 3/2\sin^2\alpha_0)/(1 - 3/4\sin^2\alpha_0)^{1/2}$. We have also assumed that the *radiation from the various tubes adds incoherently*; this is certainly reasonable on physical grounds since there is no obvious phase relationship between particles in different tubes. In fact, the beam–plasma columns corresponding to different tubes may be ejected at appreciably different times. A serious discussion of such matters would entail more detailed understanding of the nature of the spark discharges.

Finally, we sum the contributions to the radiation along $\hat{n}$ at frequency ω from field lines with *different* D. A straightforward calculation yields the following intermediate result for the total energy radiated per unit solid angle along $\hat{n}$ per unit frequency

$$\frac{d^2I_{\rm tot}}{d\omega\, d\Omega} \approx \int_{r=r_{\rm p}}^{\infty}\frac{\sin(\mu_0-\alpha_0)}{\xi_0(r,\alpha_0)}\frac{d^2I_D}{d\omega\, d\Omega}\,dr.$$

In the regime of strong coherence, $ks_0 \gg 10$ which is of interest to us, the integration is simple and yields

$$\frac{d^2I_{\rm tot}}{d\omega\, d\Omega} = \frac{4\pi n_x}{3^{10/3}\Gamma(1/3)}\left\{\frac{R^2 J_0^2(R)\, s_0(R)\,\eta_0(R)\,\xi_0(R)\,\rho_0^{1/3}(R,n_x)}{c^3 k^{2/3}}\right\}, \tag{9}$$

where $R \equiv (k_s^*)^{2/3}/(k^{2/3})\,r_{\rm p}$, $k_s^* = k^*(r = r_{\rm p})$, and $n_x = \sin\mu_0$. Using

(1) the definition of J_0 from equation (4) expressed in pulsar frame variables,
(2) the expression $\rho_0 = 4/3 r(1 - 3/4\sin^2\alpha)^{3/2}/\sin\alpha(1 - 1/2\sin^2\alpha) \approx 4/3\, r/\alpha$ when $\alpha \ll 1$,
(3) the facts that $(\eta_0\xi_0) = \eta_0(r_{\rm p})\,\xi_0(r_{\rm p})\,(r/r_{\rm p})^3$ and $n_{\rm p}(r) = n_{\rm p}(r_{\rm p})\,(r_{\rm p}/r)^3$,
(4) the definition of R in terms of k_s^*, in equation (9) we find

$$\frac{d^2I_{\rm tot}}{d\omega\, d\Omega} = \frac{2^{5/3}n_x^{2/3}}{3^{8/3}\Gamma(1/3)}\left[\frac{\gamma_\pm |e|^2 E_0'^2\, n_{\rm p}(r_{\rm p})\, A(r_{\rm p})\, s_0(R)\, r_{\rm p}^{7/3}(k_s^*)^{14/9}}{mc^3}\right]\frac{\exp(2N)}{k^{20/9}}. \tag{10}$$

The number of e-foldings between onset and time $\cong (R - r_0)/c$, N is

$$N = \frac{1}{c}\int_{r=r_0}^{r=R}\frac{dr}{\tau(r)}$$

where r_0 is onset position.

Using (m) of Table 1 to calculate N, and expressing k_s^* in terms of more fundamental

pulsar parameters, we write equation (10) as

$$\frac{d^2 I_{\rm tot}}{d\omega\, d\Omega} = \left(\frac{4}{9}\right)\left(\frac{3}{2}\right)^{1/3} \frac{n_x^{2/3}}{\Gamma(1/3)} \left\{\frac{\gamma_\pm |e|^2 E_0'^2 n_{\rm p}(r_{\rm p})\, A(r_{\rm p})\, s_0(R)\, r_{\rm p}^{7/3}}{mc^3}\right\} \frac{1}{k^{20/9}} \left[\frac{16\pi e^2 n_{\rm p}(r_{\rm p})\, \gamma_\pm}{mc^2}\right]^{7/9}$$

$$\times \left|\exp\left\{\frac{8 r_{\rm p}^{3/2}}{\gamma_{\rm b}\gamma_\pm^{1/2} c\, r_0^{1/2}} \left(\frac{\gamma_{\max}}{\gamma_\pm}\right)^{1/6} \left(\frac{\pi e B_s^d}{mcP}\right)^{1/2} \left[1 - \left(\frac{r_0}{R}\right)^{1/2}\right]\right\}\right|. \qquad (11)$$

In the Appendix we describe the origin of the factor $k^{-20/9}$ in more detail.

Equation (11) describes the spectral distribution of energy emitted into $d\Omega$ at $\hat{n}$ when *one* column of plasma moves along each tube of dimension $\xi_0 \eta_0$. The average power radiated into $d\Omega$ and $d\omega$ is

$$\frac{d^2(\text{power})}{d\omega\, d\Omega} = \left(\frac{d^2 I_{\rm tot}}{d\omega\, d\Omega}\right)(\text{number of columns emitted per tube per unit time}).$$

For continuous emission from all tubes,

$$\frac{d^2(\text{power})}{d\omega\, d\Omega} = \frac{c}{L}\left(\frac{d^2 I_{\rm tot}}{d\omega\, d\Omega}\right) \qquad (12)$$

where L is the average length of a plasma column.

Equation (12) gives the power radiated along $\hat{n}$, which is assumed fixed in the pulsar frame when **M** and $\boldsymbol{\Omega}$ are antiparallel. In a practical situation we require an expression for the average power spectrum radiated along a vector $\hat{n}_0$ fixed in space when **M** and $\boldsymbol{\Omega}$ are not parallel. We assume $\boldsymbol{\Omega}$ is fixed in space and **M** makes a constant angle Σ with respect to $\boldsymbol{\Omega}$ (see Fig. 4). The observation vector $\hat{n}_0$ is fixed in space and makes an angle β with $\boldsymbol{\Omega}$. For simplicity, assume that the polar cap remains circular and the rotational symmetry of field lines around **M** is unbroken. Hence, we need specify only θ, the angle between $\hat{n}_0$ and **M**. As **M** sweeps around $\boldsymbol{\Omega}$ at angular speed Ω, θ varies as $\cos\theta = (\sin\beta \sin\Sigma)\cos\Omega t + \cos\beta\cos\Sigma$. When $\theta \lesssim \mu_{\max}$ ($\equiv$ angular width of emission region), then equation (12) with $\mu = \theta$ describes the pulsed emission toward a distant observer along $\hat{n}_0$.

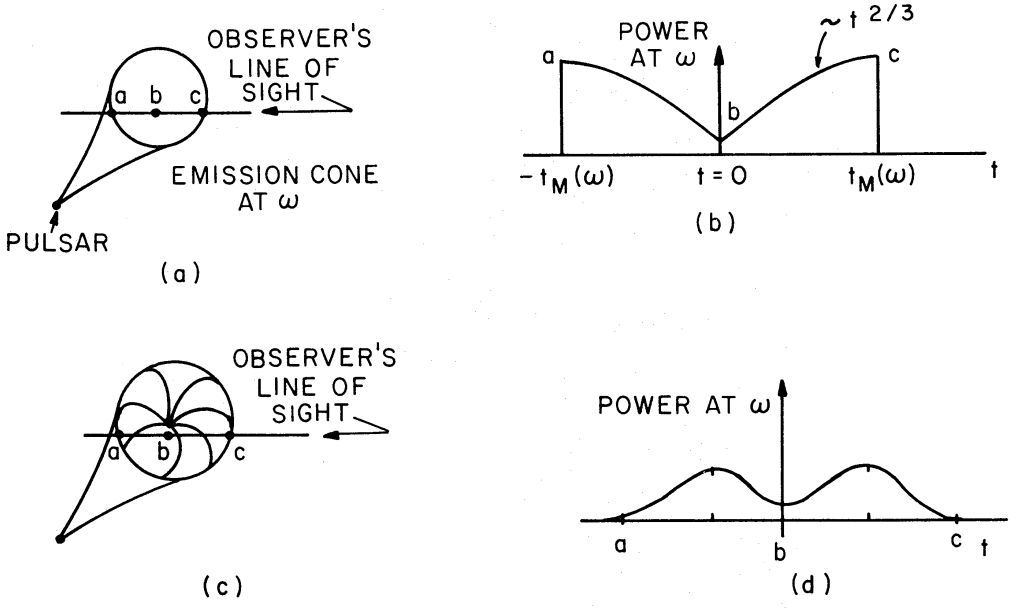

Figure 4. Trajectory of observer's line of sight (a), and (b) observed power – from equation (12) – for uniform density of radiators. If density declines at the edge of the cone, (c), power profile is smoothed in time (d).

5 Discussion of results and comparison with observations

The argument of the exponential in equation (11) is twice the number of e-foldings that occurred between onset of the instability and $r = R$. Using Table 1, letting $P = 1$ s, $r_0 = r_p$ and $R = \infty$, we find the maximum number of e-foldings to be $\approx 1/10$. Therefore, the differential emission is expected to be low unless

(a) the initial excitation level of the wave (denoted by E_0' and $s_0(r_p)$) is large or

(b) other instabilities with much higher growth rates are present. A serious discussion of (a) would require more detailed knowledge of the electrodynamics in the near magnetosphere than is currently available; case (b) we shall discuss in a future work.

5.1 LUMINOSITY

For the present we assume E_0' and s_0 are large. As the observer's line of sight sweeps across the pulsar, μ_0 and $\alpha_0(\mu_0)$ vary from a maximum value (determined by the emission cone at frequency ω) to a minimum, and back to the maximum – see Fig. 4(a). An observer fixed in space detects a pulse (at frequency ω) whose form is similar to that shown in Fig. 4(b). If the line of sight passes through the pulsar axis then the power falls to zero at $t = 0$. The sharp cutoffs in Fig. 4(b) arise if we assume a sharp boundary between open and closed field lines. Actually, we expect smearing to occur near the points $\pm t_M$ if the magnetospheric structure departs from the ideal model considered here. The diagram in Fig. 4(b) crudely explains the double-humped envelopes often observed, but does not explain the single-humped envelopes. However, if $n_p(r_p)$, say, had a significant surface angular dependence that decayed sufficiently fast toward the edge of the polar cap, then both the single and double-humped envelopes can be easily explained. Another source of smoothing in density, possibly more common, comes from noticing that field lines near the boundary between open and closed lines can be deformed by plasma pressure near the light cylinder. This may lead to lowered density along these lines and, when plasma 'loading' of these lines is included, there may indeed be no sharp boundary between the open and closed regions.

Fig. 4(c) shows a double-peacked pulse which is smoothed by the gradual decline in density toward the edges of the emitting cone.

Nevertheless, we now compare the frequency and period dependence of equation (12) with observations. We define the average differential energy observed per pulse by an observer who subtends an angle $d\Omega$ as

$$\frac{d\langle U\rangle}{d\omega} = d\Omega \left(\frac{4}{9}\right)\left(\frac{3}{2}\right)^{1/3} \frac{1}{\Gamma(1/3)} \left\{\frac{\gamma_\pm \gamma e|^2 E_0'^2 n_p(r_p) A(r_p) s_0(R) r_p^{7/3}}{mc^2 L}\right\}^{t} \left[\frac{16\pi e^2 n_p(r_p)\gamma_\pm}{mc^2}\right]^{7/9}$$

$$\times \exp\left\{\frac{8 r_p^{3/2}}{\gamma_b \gamma_\pm^{1/2} c r_0^{1/2}} \left(\frac{\gamma_{max}}{\gamma_\pm}\right)^{1/6} \left(\frac{\pi e B_s^d}{mcP}\right)^{1/2} \left[1 - \left(\frac{r_0}{R}\right)^{1/2}\right]\right\} \frac{1}{k^{20/9}} \int_{pulse} H[\mu_0(t)]\, dt \quad (13)$$

where $H[\mu_0(t)]$ is the correct angular factor, considered to be a function of time as the observer:s line of sight sweeps across the radiating region. The frequency dependence of equation (13) (neglecting any contribution from the integral) is

$$\frac{d\langle U\rangle}{d\omega} \sim \omega^{-\alpha} \quad \text{where} \quad \alpha = \frac{20}{9}. \quad (14)$$

Experimentally (Groth 1975), the spectral index α of known pulsars falls in the range $0.7 < \alpha < 3.3$ with an average value of 1.62 near $\nu \equiv \omega/2\pi \approx 400$ MHz; for the Crab pulsar

$\alpha = 2.5$. These values are quite consistent with equation (14) given the possible frequency dependence of s_0 and E_0'. At higher frequencies (~ GHz) some pulsar spectra steepen. Such a high-frequency cutoff is implicit in the exponential factor of equation (11) since $R \propto k^{-2/3}$. This exponential cutoff arises because the instability has not grown appreciably near the pulsar where the emitted frequencies are high.

Cavallo & Ventura (1972) have argued that the luminosity–period relationship can be expressed as

$$L = 1.6 \times 10^{28} \frac{1}{P(1.36^{+0.1}_{-0.2})} \text{ erg/s.} \tag{15}$$

Integration of equation (12) over solid angle and frequency allows us to estimate the luminosity–period dependence

$$P_{\text{ower}} = \left(\frac{4}{9}\right)\left(\frac{3}{2}\right)^{1/3} \frac{1}{\Gamma(1/3)} \left\{\frac{\gamma_\pm |e|^2 E_0' n_p(r_p) A(r_p) s_0(R) r_p^{7/3}}{mcL}\right\}\left[\frac{16\pi e^2 n_p(r_p)\gamma_\pm}{mc^2}\right]^{7/9}$$

$$\times 2\pi \int_{k_{\min}}^{k_{\max}} \frac{dk}{k^{20/9}} \int_{\mu_0=0}^{\mu_{0\,\max}(k,P)} \sin\mu_0 H(\mu_0)\, d\mu_0. \tag{16}$$

We discuss the low- and high-frequency cutoffs, $k_{\min}$ and $k_{\max}$, later. Using Table 1 and ignoring the period dependence of the integrals, we find Power $\propto P^{-2}$ which is higher than Cavallo's value but almost equal to the Ruderman–Sutherland estimate of $P^{-15/7}$.

High frequencies are emitted most efficiently near the star, so conditions in the near magnetosphere limit $k_{\max}$.

(*a*) A decisive cutoff is provided by the onset of the instability. Until the conditions for growth of the plasma wave are met, for $r > r_{\text{onset}}$, there is no coherence. This may be the simplest explanation for the observed high-frequency steepening in the luminosity of some pulsars. Exponential growth of the plasma wave makes the pulsar visible at high radio frequencies, and as growth proceeds the wave moves into regions further from the pulsar, for which the plasma frequency is lower. In our formulation, this appears as an $\exp(-k^{1/3})$ dependence in equation (11). Because our particular beam–plasma instability is too weak to explain the high coherence necessary, we cannot take such a detail as the $\exp(-k^{1/3})$ dependence too seriously, but it does display a fall off in frequency faster than the power law at lower frequencies as required. When the instability, whatever its detailed nature, reaches nonlinear saturation, the level of coherence will be fixed and we expect then a $\nu^{-20/9}$ dependence in $L(\nu)$, providing $s_0(\nu)$ has no frequency dependence. The fact that not all pulsars display high-frequency steepening may imply that not all have the same plasma instability, or their plasma densities, streaming velocities, etc. may differ substantially. If growth is very rapid there would be no steepening. Instead, the fully developed instability would appear at the highest observable frequencies. As an example, consider PSR 0950+08, which has a steepening of luminosity between 2 and 10 GHz (Sieber 1973). The 10-GHz point corresponds to emission from $r = 120 r_p$ above the pulsar, assuming the parameters of Table 1. This is far above the gap, and may correspond to:

(i) One species of particle overtaking another in the magnetosphere so that, when they interpenetrate, instability becomes possible.

(ii) Slow growth from the gap region outward, which becomes visible at $r = 120 r_p$.

(iii) Significant departure from dipolar fields below $120 r_p$, so that no steady conditions exist and long coherence lengths are impossible.

Deciding on (i), (ii), (iii), or some other effect depends on a better knowledge of the relevant plasma instabilities.

(*b*) The coherence length, s_0, is expected to be shorter near the star (for at least two reasons) thereby providing another high-frequency cutoff:

(1) As the unstable two-stream spectrum evolves, the width δk in k space narrows, and the length of the 'single wave' (in configuration space) increases. Near the star (and onset) we expect δk to be relatively large and s_0 small.

(2) Two particles can be coherent only if their separation is $< \rho_0/\gamma_\pm$. Near the star $\rho_0 \sim 10^6$ cm and therefore s_0 is severely limited.

Possible limits on $k_{\min}$

The problem of predicting $k_{\min}$ is equivalent to determining $r_{\max}$, the maximum distance from the pulsar at which the coherent radiation mechanism is effective.

(a) Ruderman & Sutherland predict that the beam stops feeding the instability near $r \sim 5 \times 10^9$ cm, because it outruns the plasma. However, bunching may persist because of the decay time of the mode and radiation reaction. Indeed, Goldreich & Keeley (1971) have shown that, for conditions similar to those of the Crab pulsar, appreciable particle bunching occurs solely because of radiation reaction.

(b) Onset and growth of the filamentary instability.

Beyond a certain distance from the star (to be determined below) the beam–plasma system is unstable to the filamentary instability (Benford 1976). It is a purely growing mode (Re $\omega = 0$) with $k = k_\perp$. The appropriate dispersion relation can be found from the full electromagnetic dispersion tensor in the laboratory frame (Ignat & Hirshfield 1970)

$$0 = k_\perp^2 c^2 - \omega^2 + \omega_\parallel^2 + \frac{k_\perp^2 V_p^2 \omega_{p\perp}^2}{(\omega^2 - \omega_{cp}^2)} + \frac{k_\perp^2 V_b^2 \omega_{b\perp}^2}{(\omega^2 - \omega_{cb}^2)}, \tag{17}$$

where

$$\omega_{p\perp}^2 = \frac{4\pi n_p e^2}{\gamma_\pm m}; \quad \omega_{b\perp}^2 = \frac{4\pi n_b e^2}{\gamma_b m}; \quad \omega_\parallel^2 = \frac{\omega_{p\perp}^2}{\gamma_\pm^2} + \frac{\omega_{b\perp}^2}{\gamma_b^2}; \quad \omega_{cp} = \frac{|e|B}{\gamma_\pm mc}; \quad \omega_{cb} = \frac{|e|B}{\gamma_b mc}.$$

The onset condition is found by setting $\omega = 0$ and letting n_b, n_p and B vary as $(r_p/r)^3$ in equation (17). This gives onset of instability at

$$\frac{r}{r_p} \cong \left[\frac{(B_s^d)^2}{4\pi mc^2 [n_p(r_p)\gamma_\pm + n_b(r_p)\gamma_b]} + \frac{\omega_\parallel^2(r_p)}{(kc)^2}\right]^{1/3}. \tag{18}$$

Onset depends on the net transverse pressure-like term $n\gamma mc^2$ from both beam and plasma. In fact, since $n_p = n_b(\gamma_b/2\gamma_\pm)$, the beam pressure dominates by a factor of two. The growth rate, however, is dominated by the *plasma* term. From equation (17),

$$\omega = i\left\{(\omega_{p\perp}^2 - \omega_{cp}^2) - \frac{[(\omega_{p\perp}^2 - \omega_{cp}^2) + \omega_\parallel^2]\omega_{p\perp}^2}{k^2 c^2} + O\left(\frac{1}{k^4 c^4}\right)\right\}^{1/2}. \tag{19}$$

This represents the way plasma begins to move across the magnetic field lines once the net plasma energy density exceeds the field energy density. The plasma forms filaments of electrons and positrons, which grow very quickly. The $k = \infty$ modes onset first and grow most quickly. A realistic estimate is that λ must be less than the diameter of the plasma column, d. Then $(\omega_{p\perp}/k_{\min}c) \sim 3 \times 10^{-7} d$ and for $d \ll 10^7$ cm we can neglect the k dependence of equation (19). The growth rate of (19) is r-dependent, and by integrating it from the onset point we find that the number of e-foldings $N \approx \frac{2}{3} \times 10^4 (s/r_{\text{onset}})^{3/2}$ where s is the

distance moved out from $r_{\rm onset}$. Thus the instability becomes nonlinear before the plasma has moved very far. Using $X \equiv r/r_{\rm p}$,

$$X_{\rm onset} = \left\{ \frac{\omega_{cp}^2(r_{\rm p})}{\omega_{\rm p\perp}^2(r_{\rm p})\,[1 + n_{\rm b}\gamma_{\rm b}/n_{\rm p}\gamma_{\pm}]} \right\}^{1/3}. \tag{20}$$

From Table 1, $n_{\rm b}\gamma_{\rm b}/n_{\rm p}\gamma_{\pm} \leqslant 2$. The observed coherent radiation frequency at $r_{\rm onset}$ is

$$\nu_{\rm obs}(r_{\rm onset}) = \frac{\gamma_{\pm}}{\pi}\,\omega_{\rm p\perp}(r_{\rm p})\,\frac{1}{X_{\rm onset}^{3/2}}$$

$$= 10^7 \rho_6^{4/7} P^{-8/7} B_{12}^{-1/7}/{\rm s}, \tag{21}$$

and

$$r_{\rm onset} = r_{\rm p}\, 6.8 \times 10^3 B_{12}^{8/21} P^{8/21} \rho_6^{-4/21}$$

when $\gamma_{\rm b} = \gamma_{\rm max}$.

For pulsars with $P \lesssim 0.2$ s, $\nu_{\rm obs}$ falls into the 100-MHz range. We cannot, though, take equation (21) as a precise calculation of the frequency at which the radio luminosity should turn over and begin its decline, because (1) radiation may not cease quickly after filaments form, and (2) the field lines are pushed about by the plasma pressure, so the radius of curvature of the lines and the plasma density may change quickly after onset. Reason (1) follows because electrostatic bunching with $k = k_z$ may not be immediately disturbed by magnetostatic pinching ($k = k_\perp$), since coupling occurs only through the perturbations on the particle orbits.

There is a further difficulty. Thus far we have not considered the orientation of the angular momentum vector $\boldsymbol{\Omega}$ and $\mathbf{B}$. If $\boldsymbol{\Omega}$ is parallel to $\mathbf{B}$ the field pattern is undisturbed high over the polar cap, and the radio radiation and filamentation occur before the field lines curve over to intersect the light cylinder ($\theta \ll 1$). But if $\boldsymbol{\Omega}$ is normal to $\mathbf{B}$, at a distance $R_{\rm L} = cP/2\pi$ above the cap the light cylinder destroys the dipolar field. Using equation (20) and Table 1, we find

$$\frac{r_{\rm onset}}{R_{\rm L}} = 1.42\, P^{-13/21} B_{12}^{8/21} \rho_6^{-4/21}. \tag{22}$$

Taking

$$B_{12} = 1,\ \rho_6 = 1,\ r_{\rm onset} < R_{\rm L} \quad \text{when} \quad P > 1.76\ {\rm s}.$$

If we knew the Ruderman–Sutherland model were very accurate we could conclude that only long-period pulsars in the $\boldsymbol{\Omega} \perp \mathbf{B}$ mode can show turnover. But allowing for uncertainties, it is probable that equation (22) gives no true test. The same may be said of the period dependence of equation (21). Sieber's data (1973) show only a slow decline in $P(\propto P^{-1/2})$. For a discussion of the nonlinear and other aspects of filamentary instabilities, see Benford (1973, 1976).

The conventional explanation of the low-frequency turnover is self-absorption (Sieber 1973). This view has not been explored for coherent radiation; existing models apply to incoherent emission in weak magnetic fields. Simply assigning a brightness temperature of $\delta n_{\rm p}\gamma_{\pm}mc^2$ will give a turnover and a power-law slope ν^2. Deciding between the filamentation explanation and self-absorption depends on a better fix on magnetospheric quantities.

5.2 RADIATION DAMPING

We have used the two-stream growth rate without including the effect of the electromagnetic radiation back upon the beam–plasma system. This neglects the radiation instability of Goldreich & Keeley (1971) and the assertion by Hinata (1976) that the radiation losses completely damp the two stream instability.

The Hinata argument rests on his energy balance equation, which assumes that the wave energy grows at the linear growth rate and is damped by the total loss rate of the beam–plasma system through curvature radiation. But this is only true if the energy for radiation is provided solely by the electrostatic waves. This is not so. Instead, the process resembles a laser, in which an incoherent emission process is ordered by a stimulus. The energy invested in the coherence-producing effect can be quite small; it merely triggers the amplification of a pre-existing incoherent mechanism, and thus taps a much larger energy reservoir. The point here is that the electrostatic wave grows because of the free energy available in the *beam*, and the electromagnetic radiation is emitted by the plasma; there are two different agencies involved. Equating loss and gain rates only makes sense when these rates apply to the same physical system.

Further, Hinata's calculation assumes the appropriate radiation rate is proportional to γ_w^4, when in fact the plasma particles which are emitting do not have the same energy factor as the electrostatic wave ($\gamma_\pm \approx 800$, $\gamma_w \sim \gamma_b \approx 10^6$).

Finally, the study by Goldreich & Keeley (1971), which treats the electromagnetic field precisely and uses linearized fluid equations, shows that the net effect of radiation can augment instability. Their growth rate,

$$\gamma^* \approx \frac{c}{\rho}\left(\frac{N_0 e^2}{mc^2 \gamma_\pm^3 \rho}\right)^{1/2},$$

where N_0 is the number of particles along a field line, can give a growth rate $\sim 10^2 c/\rho$ for reasonable pulsar parameters, and thus could conceivably be the principal agency producing coherence. We hope to include the effects treated by Goldreich & Keeley in a more detailed model of the pulsar magnetosphere in a future work, to determine whether this radiation instability can dominate over the effects of the electrostatic streaming instability.

Our conclusion is that, rather than damping instabilities, radiation may enhance it. In this sense our result for the luminosity may be a conservative estimate, as long as we use only the conventional plasma growth rates. Since electrostatic modes are typically rapidly growing, we must be sure none exist before we invoke the somewhat slower Goldreich–Keeley mechanism.

6 Conclusions

We have pursued a model of coherent emission based on the arranging of particles by an instability, so that radiation was correlated over many wavelengths. This depends on the single-wave model, i.e. a sharp peak in k_z-space. This phased array picture, in which the plasma becomes an extended antenna, is much more efficient than the conventional view of coherence. When the single-wave model breaks down, the free energy available for the instability will remain, forcing coherence in local groupings. We contrast the two pictures with a simple scaling argument. For the phased array, the number of cooperating particles is the number of bunched particles within a wavelength, N, times the number of such lengths in the 'antenna' of length s_0, s_0/λ. Then the coherent power for the antenna model is $P_a \propto (Ns_0/\lambda)^2$. When the single-wave model fails, the localized clumps will be correlated only

over distances of size λ. If we suppose the number of particles in a wavelength is still N, then the radiation power is proportional to N^2 times the number of bunches, N^*. Just after the phased array has broken up, it seems reasonable to guess that $N^* \sim s_0/\lambda$. Then the power from these bunches is $P^* \propto N^2 s_0/\lambda$ and

$$\frac{P_a}{P^*} \sim \frac{(N s_0/\lambda)^2}{N^2 s_0/\lambda} = \frac{s_0}{\lambda} \gg 1.$$

Thus the phased array produces much more power than a turbulent wave spectrum. The transition from P_a to P^* may be the cause of low-frequency turnover in spectra, perhaps hastened by onset of filamentation instability. If decay of single-wave coherence occurs early, it could be that all the pulsar radiation comes from localized modes. If so, the luminosity function, equation (11) will be altered by a reduction of magnitude $\sim \lambda/s_0$.

Because the beam–plasma instability of Ruderman & Sutherland fails to yield significant coherence, some (perhaps extensive) changes will be necessary to explain the radiation. This paper's formalism will still apply, with suitable alterations, so long as the plasma wave velocity is relativistic in the plasma frame.

If this is *not* so, our alternate forms for the luminosity, involving the customary single-particle functions, should be used (Buschauer & Benford 1976). Before such cases can be worked out, though we must have a better understanding of the pulsar magnetosphere.

Table 2.

Quantity	Relation
Filamentation onset point★	$r = \frac{9.8 \times 10^3}{(1+\epsilon)^{1/3}} r_p B_{12}^{8/21} P^{8/21} \rho_6^{-4/21}$
Distance from pulsar where frequency ν is emitted	$R(\nu) = 3.2 \times 10^8 r_p \nu^{-2/3} \rho_6^{4/21} B_{12}^{2/7} P^{-8/21}$
Observed ν in terms of plasma density	$\nu = \frac{\gamma_\pm^{1/2}}{\pi} \left(\frac{4\pi n_p e^2}{m}\right)^{1/2}$
Frequency at onset of filamentation	$\nu = 10.4 \rho_6^{4/7} B_{12}^{-1/7} P^{-8/7}$ MHz

Notes:

★ $\epsilon \equiv n_b \gamma_b / n_p \gamma_\pm$ is not completely determined in the model; $2/3 \lesssim \epsilon \lesssim 2$.

We have tried to make our results accessible to the observing community by providing Tables 1 and 2, which give convenient conversions from observed radiation properties to pulsar parameters (r, B, n_p, etc.). We hope these will ease comparison with observations. However, since the basis for these tables is the Ruderman–Sutherland model, which is probably invalid at least in detail, the overall success of our radiation formulae cannot be equated with the tables.

The principal observational consequences of our calculations are:

(1) Equation (11) for the luminosity, which awaits a better (and larger) expression for the growth rate in the exponential. The $\nu^{-2.2}$ dependence can be modified if $s_0 = s_0(\nu)$, as seems likely (see Appendix). Also, the $\theta^{2/3}$ dependence differs from the single-particle result. Fig. 6 displays some of our ideas about how plasma mechanisms influence the luminosity.

(2) $L(P) \propto P^{-2}$.

(3) Low-frequency turnover in the spectrum may arise when, at a point $\geq 10^9$ cm from the pulsar, the relativistic plasma energy density exceeds the dipolar field energy density.

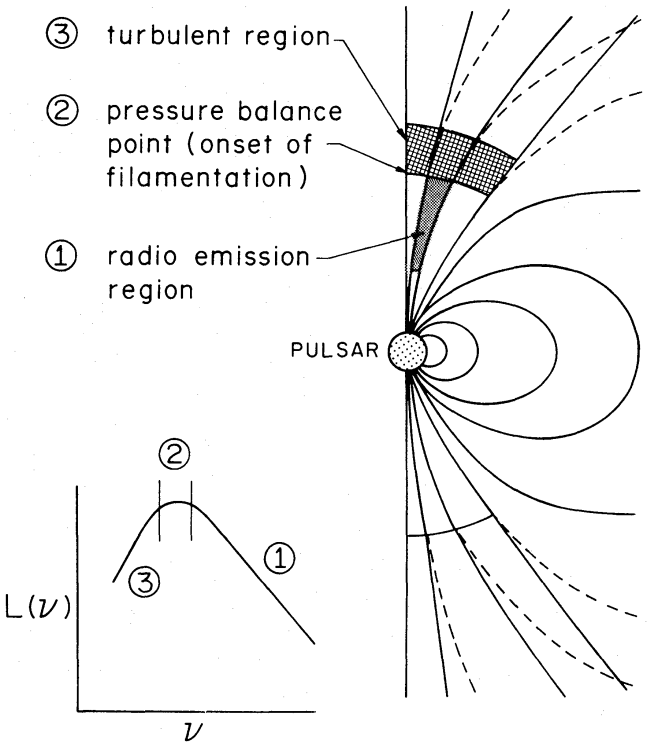

Figure 5. Relation between spatial regions and frequency spectrum. The pressure balance point corresponds to turnover in luminosity, $L(\nu)$.

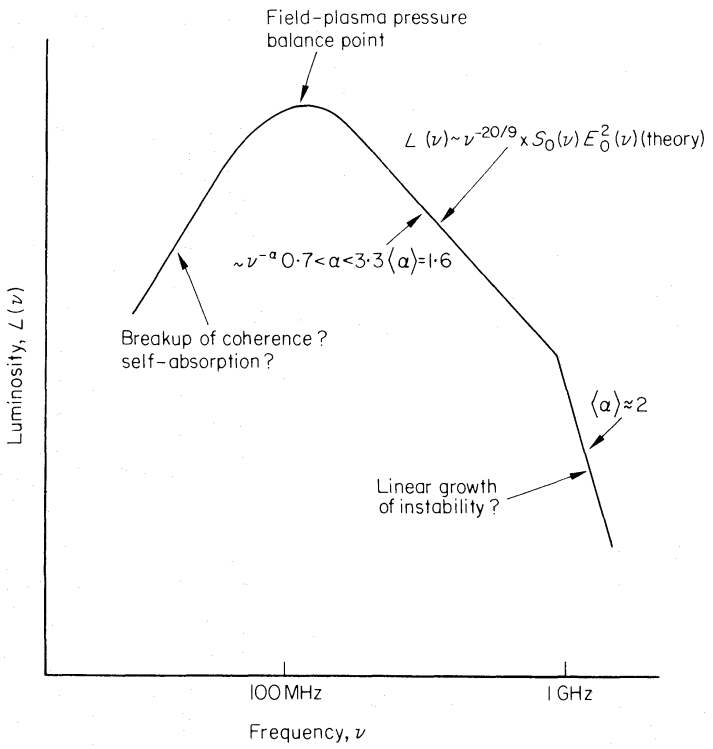

Figure 6. Analysis of a 'typical' pulsar luminosity spectrum. Observed α lies between 0.7 and 3.3 for the middle power law region, and observed $\langle\alpha\rangle \approx 2$ for the steepening.

(Table 2, equations (17) to (22), and Fig. 5). This may explain some features of 25-MHz radiation. It would be interesting to see if similar structure prevails over a broader range of very low frequencies.

Acknowledgments

This work was supported by a grant from the National Science Foundation, Grant No. MPS75-14625. One of us (GB) acknowledges stimulating conversations with B. Rickett, V. Trimble, J. Aarons, C. Max, D. Backer and M. Ruderman.

Appendix

Frequency dependence of the luminosity

In this Appendix we consider the contributions to the frequency dependence of equation (10). In the regime of strong coherence and angle $\alpha_0 \ll 1$, radiation at wavenumber k is emitted from the vicinity of $r = R \equiv (k_s^*)^{2/3} r_p k^{-2/3}$. This relation allows us to replace the R dependence in equation (9). A factor $k^{1/3}\rho_0^{1/3}\alpha k^{1/3} R^{1/3} \alpha k^{1/9}$ comes from the single particle radiation term in equation (7). However, if the phase velocity of the wave in the plasma frame is $\ll c$, the above $k^{1/9}$ dependence would be replaced by $k^{1/3}$ times the k-dependence of a Bessel function (Buschauer & Benford 1976). The integration over tubes (r integration) contributes a term proportional to $R^2/k \propto k^{-7/3}$ and the diverging tubes themselves contribute a term $\xi_0\eta_0)_{r=R} \propto \xi_0\eta_0)_{r=r_p} R^3 \propto k^{-2}$. Therefore, *the k dependence which is independent of the exact form of the instability* (except for the weak wave phase velocity effect discussed above) is $k^{1/9}k^{-2}k^{-7/3} = k^{-38/9}$. The precise form of the instability defines J_0^2 and for the streaming instability $J_0^2 \propto n_b(R) \propto R^{-3} \propto k^2$. The total k dependence is, of course, $k^{-38/9+2} = k^{-20/9}$. Note that we have ignored the k dependence of the exponential factor in equation (10) and s_0. The former is proportional to $\exp(-Ak^{1/3})$ where $Ak^{1/3} \ll 1$ due to the slow growth of the instability. Presumably, for a rapidly growing mode which reaches saturation, $E^2 s_0$ will have some k dependence which can be calculated. Suppose the saturated amplitude is of the form

$$E^2 = Q n_b \gamma_b mc^2,$$

where Q is a constant independent of k. This is a fairly common form (Thode, private communication). Then since $n_b(R) \propto R^{-3} \propto k^2$, the luminosity will scale as $k^{-20/9} s_0(k)$.

Of course, s_0 is an average property of the coherence. Many complicated effects are buried in it, so making a simple choice which reliably 'predicts' observations is probably impossible.

References

Benford, G., 1973. *Plasma Phys.*, **15**, 483.
Benford, G., 1976. *Astr. Astrophys.*, **47**, 203.
Buschauer, R. & Benford, G., 1976. *Mon. Not. R. astr. Soc.*, **177**, 109.
Cavallo, G. & Ventura, A., 1972. *Astr. Astrophys.*, **18**, 287.
Ginzburg, V. L. & Zheleznyakov, V. V., 1975. *A. Rev. Astr. Astrophys.*, **13**, 511.
Godfrey, B. B., Shanahan, W. R. & Thode, L. E., 1975. *Phys. Fluids*, **18**, 346
Goldreich, P. & Keeley, D. A., 1971. *Astrophys. J.*, **170**, 463.
Groth, E. J., 1975. *Neutron stars, black holes and binary X-ray sources*, p. 119, eds H. Gursky & R. Ruffini, D. Reidel Publ. Co., Dordrecht, Holland.
Hinata, S., 1976. *Astrophys. J.*, **203**, 223.

Holloway, N. J., 1975. *Mon. Not. R. astr. Soc.*, **171,** 619.
Ignat, D. W. & Hirshfield, J. L., 1970. *Phys. Rev. A,* **1,** 872.
Jackson, J. D., 1962. *Classical electrodynamics,* John Wiley & Sons, Inc., New York.
Mikhailovskii, A. B., 1974. *Theory of plasma instabilities,* Vol. I, Plenum Publ. Co., New York.
Ruderman, M. A. & Sutherland, P. G., 1975. *Astrophys. J.*, **196,** 51.
Sieber, W., 1973. *Astr. Astrophys.*, **28,** 237.
Sturrock, P. A., 1971. *Astrophys. J.*, **164,** 529.
Thode, L. E., 1973. *PhD thesis,* Cornell University.